

Optical Tamm states enhanced broad-band absorption of organic solar cells

Xu-Lin Zhang, Jun-Feng Song, Xian-Bin Li, Jing Feng, and Hong-Bo Sun

Citation: [Applied Physics Letters](#) **101**, 243901 (2012); doi: 10.1063/1.4770316

View online: <http://dx.doi.org/10.1063/1.4770316>

View Table of Contents: <http://scitation.aip.org/content/aip/journal/apl/101/24?ver=pdfcov>

Published by the [AIP Publishing](#)

Articles you may be interested in

[Fano-induced solar absorption enhancement in thin organic photovoltaic cells](#)

Appl. Phys. Lett. **105**, 141118 (2014); 10.1063/1.4898011

[Highly transparent Nb-doped indium oxide electrodes for organic solar cells](#)

J. Vac. Sci. Technol. A **32**, 021202 (2014); 10.1116/1.4832238

[Optical and carrier transport properties of graphene oxide based crystalline-Si/organic Schottky junction solar cells](#)

J. Appl. Phys. **114**, 234506 (2013); 10.1063/1.4847515

[Broadband light trapping in thin organic photovoltaic cells using plasmonic resonant antennas](#)

J. Appl. Phys. **114**, 084504 (2013); 10.1063/1.4817369

[Origin of the enhanced performance in poly\(3-hexylthiophene\): \[6,6\]-phenyl C 61 -butyric acid methyl ester solar cells upon slow drying of the active layer](#)

Appl. Phys. Lett. **89**, 012107 (2006); 10.1063/1.2212058

The advertisement features a 3D simulation of a cylindrical component with a red and yellow heat map overlay, indicating a simulation of heat or stress distribution. The text 'Over 600 Multiphysics Simulation Projects' is prominently displayed in white and blue. A blue button with the text 'VIEW NOW >>' is located in the bottom right corner. The COMSOL logo is also present in the bottom right corner.

Over **600** Multiphysics Simulation Projects

[VIEW NOW >>](#)

COMSOL

Optical Tamm states enhanced broad-band absorption of organic solar cells

Xu-Lin Zhang,¹ Jun-Feng Song,^{1,2,a)} Xian-Bin Li,¹ Jing Feng,¹ and Hong-Bo Sun^{1,a)}

¹State Key Laboratory on Integrated Optoelectronics, College of Electronic Science and Engineering, Jilin University, 2699 Qianjin Street, Changchun 130012, China

²Institute of Microelectronics, A*STAR (Agency for Science, Technology and Research), 11 Science Park Road, Singapore Science Park II, Singapore 117685

(Received 25 September 2012; accepted 26 November 2012; published online 11 December 2012)

We present a design concept of thin-film organic solar cells using a photonic crystal as the electrode. Through the excitation of optical Tamm states (OTSs), the proposed photonic crystal based organic solar cells (PC-OSCs) exhibit a broad-band absorption enhancement owing to the abnormal refractive index variation of the active layer. The overall absorptivity can be increased by ~35% compared with that of the optimized conventional planar OSC. Remarkably, our easily manufactured planar PC-OSC exhibits almost the same overall absorptivity as the optimized conventional corrugated OSC. The excellent performance comes from the achievement of OTS for both transverse-magnetic and transverse-electric polarized enhanced absorption. © 2012 American Institute of Physics. [<http://dx.doi.org/10.1063/1.4770316>]

Organic solar cells (OSCs) based on conjugated polymers and small molecules have been attracting more and more attention due to their merits of low cost, ease of room-temperature manufacturing, light weight, and mechanical flexibility.¹⁻³ In polymer solar cells, polymer-fullerene bulk heterojunctions have been employed to overcome the exciton diffusion bottleneck. Yet there is still a tradeoff between the photon absorption efficiency and the extraction of charge carriers, as the active layer is typically required to be less than 100 nm in view of the low carrier mobility, and that greatly limits the efficiency of incident light absorption.⁴ In order to improve the photon absorption, advanced photon management designs have been proposed, such as those by the excitations of propagating surface plasmon polaritons (SPPs) and localized SPP through introducing periodically nanopatterned metal films⁵⁻⁷ and metallic nanoparticles,⁸ respectively. Although photon absorption enhancement has been achieved, it requires complicated micro-nanofabrication processes,⁹ in which the introduction of nanopatterned structures may meanwhile result in degradation of the electrical performance of the devices.¹⁰ Moreover, the absorption bandwidth of the SPP is relatively narrow,⁶ and only the absorption of transverse-magnetic (TM) polarized incidence can be enhanced.⁷ Therefore, a way of broad-band dual-polarized absorption enhancement is urgently desired in present OSCs.

Recently, a type of surface waves named optical Tamm states (OTSs) was discovered at metal/photonic crystal (PC) interface.¹¹ Such OTS exhibit local maximum field intensity at the metal/PC interface. The field intensity decays into the PC due to the Bragg forbidden band effect. In contrast to the only TM-polarized SPP, both TM and transverse-electric (TE) polarized OTS exist. Moreover, they can be excited directly from free space incidence without the assistance of nanopatterned structures. Owing to these superiorities, OTS show great potential as an alternative photon management method. Specifically, through the excitation of OTS in

OSCs, more photons would be harvested near the metal/PC interface due to the characteristics of the surface wave. Therefore, the active layer should be laid near the metal/PC interface. In spite of the aforementioned advantages, such excitation of OTS requires a fabrication of multiple PC bilayers with a precise control of lattice thicknesses, which may be more complicated than the fabrication of nanopatterned structures. In our present study, we will show in fact only two PC bilayers are sufficient for the OSCs, which could simplify the fabrication process.

In this work, we theoretically investigate the possibility of introducing OTS into OSCs to achieve a broad-band absorption enhancement. The OTS have not been applied in OSCs for photon absorption enhancement. Our study is inspired by the work of Puzzo *et al.*¹² that photonic crystals can be used as electrodes in organic light emitting devices (OLEDs). By introducing only two PC bilayers, the designed photonic crystal based organic solar cell (PC-OSC) exhibits a broad-band absorption enhancement in the active layer with ~35% higher overall absorptivity than that of the optimized conventional OSC. The broad-band absorption enhancement can be partly attributed to the abnormal refractive index (RI) variation of the active layer, which is confirmed by our theoretical model. Remarkably, the performance of the proposed planar PC-OSC is almost as well as the one of an optimized conventional corrugated OSC with a proper chosen grating period.

We study polymer based OSCs with poly-3-hexylthiophene-phenyl-C61-butyric (P3HT:PCBM) as active layers in this work. A schematic of the designed PC-OSC is shown in Fig. 1(a), where n_{PC} denotes the number of PC bilayers. The active layer P3HT:PCBM is also considered as half a PC bilayer due to its high RI for the formation of OTS.¹¹ The PC bilayer consists of periodically alternating layers of tin-doped indium oxide (ITO) and antimony-doped tin oxide (ATO) with their thicknesses of d_1 and d_2 , respectively.¹² An ultra-thin active layer is chosen with its thickness of 40 nm throughout this study. The conventional Ag/P3HT:PCBM/ITO OSC⁶ is also investigated for reference as shown in Fig. 1(b) with

^{a)} Authors to whom correspondence should be addressed. Electronic addresses: songjf@ime.a-star.edu.sg and hbsun@jlu.edu.cn.

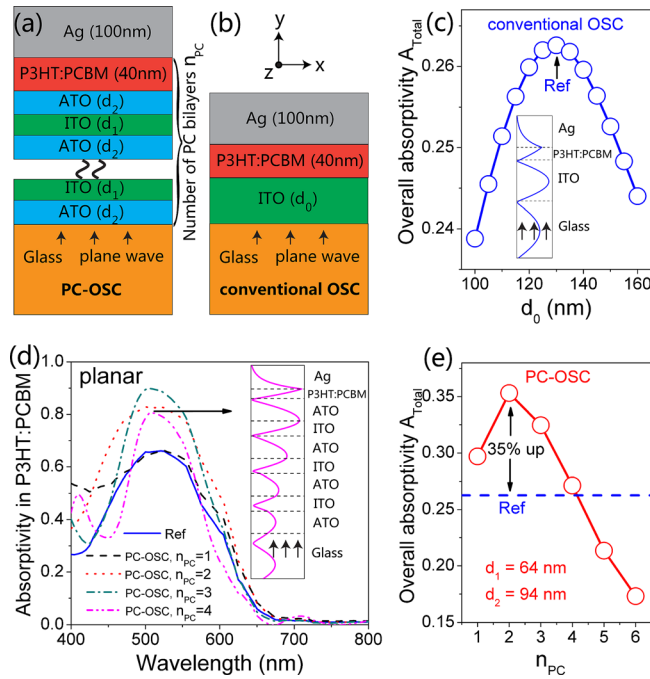


FIG. 1. Schematic of the designed PC-OSC (a) and the conventional OSC (b). (c) Calculated overall absorptivity A_{Total} of the conventional planar OSC as a function of the ITO thickness, where the OSC exhibiting the largest overall absorptivity with the ITO thickness of 130 nm is denoted as the reference OSC. (d) Simulated absorptivity spectra in the P3HT:PCBM layer of the planar PC-OSC for normal TM-polarized incidence with different number of PC bilayers. In the calculations, the lattice parameters are chosen as $d_1 = 64$ nm and $d_2 = 94$ nm. The absorptivity spectra of the planar reference OSC is also given by the blue solid line. (e) Calculated overall absorptivity A_{Total} of the planar PC-OSC as a function of the number of PC bilayers, where the PC-OSC with two PC bilayers exhibits an overall absorptivity of $\sim 35\%$ higher than the reference OSC.

the ITO thickness of d_0 . In-house generated finite-difference time-domain (FDTD) codes¹⁰ are applied to simulate the absorptivity spectra in the active layer. The Drude model is chosen to deal with Ag in the FDTD simulation. We choose the RIs of P3HT:PCBM, ITO, and ATO from Refs. 13, 14, and 12, respectively. We use the TM total absorptivity A_{TM} , TE total absorptivity A_{TE} , and overall absorptivity A_{Total} as criteria for the performance of the OSC.⁷ They are calculated

$$\text{by } A_{TM,TE} = \frac{\int_{400\text{nm}}^{900\text{nm}} a_{TM,TE}(\lambda) S(\lambda) d\lambda}{\int_{400\text{nm}}^{900\text{nm}} S(\lambda) d\lambda} \text{ and } A_{Total} = \frac{A_{TM} + A_{TE}}{2},$$

where $a_{TM,TE}(\lambda)$ are the absorptivity spectra in the P3HT:PCBM layer for TM- and TE-polarized incidence, respectively, and $S(\lambda)$ is the solar irradiance spectrum under AM1.5 illumination.⁷ In this study, we only consider the case of normal incidence. For planar structures under normal incidence, we have $A_{TM} = A_{TE} = A_{Total}$.

We first optimize the conventional OSC shown in Fig. 1(b) to find its best performance. The result is given in Fig. 1(c) for the normal incidence. It is shown that the structure exhibits the largest overall absorptivity A_{Total} (~ 0.263) with the ITO thickness of 130 nm, which is due to the good matching of the cavity mode peak in ITO (~ 520 nm) with the absorptivity peak of P3HT:PCBM (~ 502 nm). The inset of Fig. 1(c) gives the H_z field amplitude distributions with the wavelength of 520 nm for TM polarization. Hereafter, we denote the conventional OSC with the ITO thickness of 130 nm as the reference OSC.

We then investigate the active layer absorptivity spectra and the overall absorptivity A_{Total} of the designed PC-OSC by changing the number of PC bilayers n_{PC} . The results are shown in Figs. 1(d) and 1(e) with $d_1 = 64$ nm and $d_2 = 94$ nm for normal incidence. The results for TM and TE polarization are the same, and we only show the TM result in Fig. 1(d). The reason of the choice for d_1 and d_2 will be discussed later. We observe from Fig. 1(e) that the best performance of the PC-OSC is obtained with two PC bilayers, where the overall absorptivity (~ 0.353) exhibits a $\sim 35\%$ enhancement compared with the reference OSC (~ 0.263). By comparing the best PC-OSC (red dotted line) with the reference OSC (blue solid line) in Fig. 1(d), a broad-band absorption enhancement in the active layer is confirmed due to the excitation of broad-band OTS in the designed device. However, as the number of PC bilayers increases further, the overall absorptivity decreases. This is due to the narrowing bandwidth of OTS with more PC bilayers as shown in Fig. 1(d). Here the TM-polarized H_z field amplitude distributions at wavelength of 510 nm with $n_{PC} = 4$, corresponding to its absorption peak, is shown in the inset of Fig. 1(d). From the figure, the excitation of the OTS is confirmed, with the field peaking at the Ag/PC interface and exhibiting an oscillating-damping profile into the PC.

Next, we fix $n_{PC} = 2$ for the largest overall absorptivity, to investigate the dependence of the overall absorptivity on the PC lattice parameters. Figure 2(a) illustrates the overall absorptivity A_{Total} as a function of different combinations of d_1 and d_2 , where the blue star represents the designed PC-OSC exhibiting the best performance with $d_1 = 64$ nm and $d_2 = 94$ nm. The achievement of such performance is partly due to that OTS wavelength is close to the absorptivity peak of P3HT:PCBM. Here, the OTS wavelength is essentially the one at which the wave vector of the eigenmode is zero, as we deal with the case of normal incidence.¹¹ However, we remark that the larger OTS bandwidth induced broad-band absorption enhancement (see $n_{PC} = 2$ in Fig. 1(d)) is the most crucial factor for the best performance. We attribute such larger OTS bandwidth to (1) the fewer PC bilayers, which could be better understood by comparing the absorptivity spectra under different PC bilayers in Fig. 1(d), and (2) very significantly, the abnormal RI variation of P3HT:PCBM, which will be discussed below in detail.

To illustrate the second point clearly, we calculate the OTS wavelength λ_{OTS} as a function of different active layer thicknesses d_a , as shown by the red-circle-line in Fig. 2(b). In the calculation, the absorptivity peak of the whole structure is considered as the OTS wavelength, where the extinction coefficient of the active layer is omitted in order to make the peak clearly. We define $f(d_a)$ as the derivative of the OTS wavelength towards the active layer thickness: $f(d_a) = \frac{\partial \lambda_{OTS}}{\partial d_a}$. It is noted from Fig. 2(b) that $f(d_a)$ exhibits a suddenly increase in the wavelength range 520–560 nm, as marked by the red dashed circle. One can see that if we choose an active layer thickness within this abnormal region, e.g., 40 nm in the designed PC-OSC, more wavelengths would satisfy or nearly satisfy the OTS condition. Therefore, the OTS bandwidth would become larger. We will show that the origin of this abnormal region comes from the abnormal RI variation of P3HT:PCBM in the same wavelength range

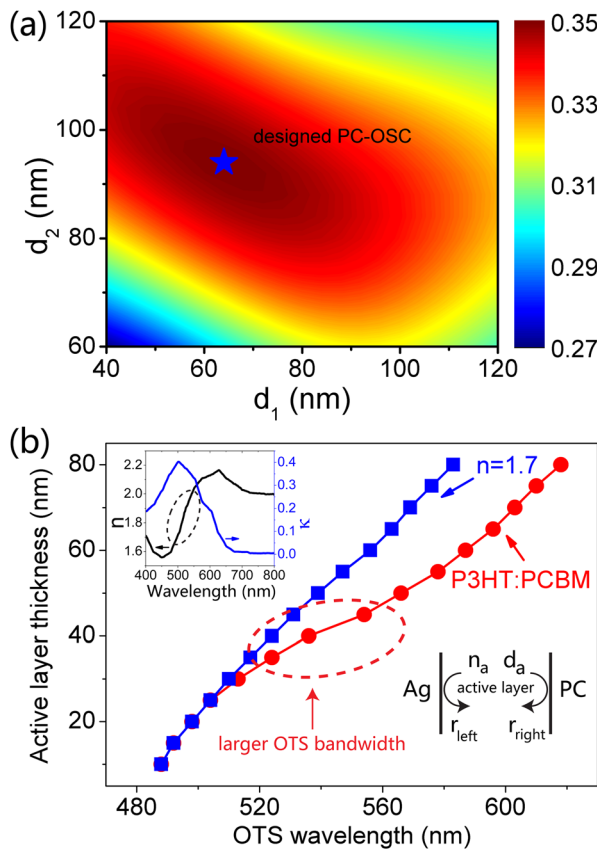


FIG. 2. (a) Calculated overall absorptivity A_{Total} of the planar PC-OSC with two PC bilayers as a function of different combinations of d_1 and d_2 . The blue star represents the designed PC-OSC ($d_1 = 64$ nm, $d_2 = 94$ nm) discussed in this work. (b) Calculated OTS wavelength as a function of the active layer thickness, where the active layer is chosen as P3HT:PCBM (red-circle-line) or a layer with $RI = 1.7$ (blue-square-line). The red dashed circle indicates the region with the larger OTS bandwidth. The insets show the RI of P3HT:PCBM and the theoretical model for the analysis of the larger OTS bandwidth (see Eq. (1)).

(520–560 nm), which is shown by the inset of Fig. 2(b). We observe that in this wavelength range, the refractive index (n) exhibits an abnormal increase with the increase in wavelength (black dashed circle), where the extinction coefficient (κ) is around its maximum. In this work, such RI variation is called as an abnormal RI variation. This is in contrast to the normal RI variation, which can be expressed by the well-known Drude model.

To reveal the relation between $f(d_a)$ and the RI variation, we present a theoretical deviation of $f(d_a)$, by following the theory in Ref. 11. The model is shown in the inset of Fig. 2(b). Here, taking TE polarization for instance, the OTS condition can be written as

$$\varphi(r_{left}) + \varphi(r_{right}) + 2\varphi_a = 2m\pi, \quad (1)$$

where φ demonstrates the phase, r_{left} and r_{right} are the amplitude reflection coefficient, $\varphi_a = 2\pi n_a d_a / \lambda_{OTS}$, n_a is the RI of the active layer, and m is an integer. By substituting $r_{left} \approx \exp\left[i\left(\pi + \frac{2n_a\omega_{OTS}}{\sqrt{\epsilon_b}\omega_p}\right)\right]$ and $r_{right} \approx \exp\left[i\beta\left(\frac{\omega_{OTS}-\omega_B}{\omega_B}\right)\right]$ (Ref. 11) into Eq. (1), where ω_{OTS} , ω_B , ϵ_b , and ω_p stand for the OTS frequency, Bragg frequency, infinite frequency permittivity, and plasma frequency for Ag, respectively, and $\beta = \pi n_{ITO} / (n_{ITO} - n_{ATO})$, the OTS wavelength is obtained as

$$\lambda_{OTS} = \left[\lambda_B + \frac{4\pi n_a c}{\beta} \left(\frac{1}{\sqrt{\epsilon_b}\omega_p} + \frac{d_a}{c} \right) \right] / \left(1 - \frac{\pi}{\beta} \right), \quad (2)$$

where c is the vacuum light speed. Notice in Eq. (2), n_a is a function of λ_{OTS} , thus we have

$$f(d_a) = \frac{\partial \lambda_{OTS}}{\partial d_a} = \frac{n_a/c}{\frac{\beta - \pi}{4\pi c} - \frac{\partial n_a}{\partial \lambda_{OTS}} \left(\frac{1}{\sqrt{\epsilon_b}\omega_p} + \frac{d_a}{c} \right)}. \quad (3)$$

From Eq. (3), we find that $f(d_a)$ would become larger if $\frac{\partial n_a}{\partial \lambda_{OTS}} > 0$, corresponding to a region where the RI increases as the wavelength increases. This indicates that the larger bandwidth of OTS in the designed PC-OSC is partly due to the abnormal RI variation of P3HT:PCBM, as usually the organic materials exhibit a decreasing RI with the increase in wavelength in the visible range. As a contrast, we calculate the OTS wavelength as a function of d_a with an active layer exhibiting $RI = 1.7$. The result is given by the blue-square-line in Fig. 2(b), from which the aforementioned abnormal region no longer exists, thus the bandwidth would not be extended.

We then investigate the corrugated PC-OSC integrated with 40 nm-height wavelength-scale periodic gratings^{15,16} in order to further improve the performance of the PC-OSC. Compared with the planar one, a larger overall absorptivity is expected due to the excitation of SPP waves for TM-polarized incidence. In the calculations, the structure parameters of the PC-OSC are remained the same as $n_{PC} = 2$, $d_1 = 64$ nm, and $d_2 = 94$ nm. The normal incidence absorptivity spectra in the active layer are shown in Figs. 3(a) and 3(b) for TM and TE polarization, respectively. Here, the cases of the planar reference OSC and the planar PC-OSC are also shown for comparison. For TM polarization, the propagating SPP waves at the Ag/P3HT:PCBM interface can be excited through the diffraction of the grating associated with an enhanced absorption.⁶ This is confirmed by the peak of 715 nm with a period $\Lambda = 360$ nm in Fig. 3(a), with its H_z field amplitude distributions shown in Fig. 3(d). For a smaller period (e.g., 200 nm), the SPP peak is not obvious, however, the absorptivity spectrum exhibits a broad-band absorption enhancement compared with the planar PC-OSC. We give an approximate calculation to explain this broad-band enhancement, which is also due to the abnormal RI variation of P3HT:PCBM. Here, we calculate the effective refractive index n_{eff} (Ref. 17) of the SPP waves at the Ag/P3HT:PCBM interface as a function of wavelength simply by $n_{eff} = \sqrt{\frac{n_{Ag}^2 n_a^2}{n_{Ag}^2 + n_a^2}}$.¹⁸ Then the period can be calculated as a function of the SPP wavelength from the grating diffraction equation $n_{eff}\Lambda = \lambda_{SPP}$ (normal incidence, first order diffraction).¹⁰ The result is shown in the inset of Fig. 3(a) that multiple SPP peaks may come out with a proper chosen period, such as ~ 225 nm (red dashed line). This is a result of the abnormal RI variation of P3HT:PCBM, where n_{eff} increases as the wavelength increases. For TE polarization, it is noted from Fig. 3(b) that the spectra of PC-OSC with gratings exhibit almost the same characteristics as the planar one, except some minor fluctuations. From the field point of view, the dip of $\lambda = 465$ nm in the case of $\Lambda = 280$ nm can be attributed to the ITO waveguide mode as demonstrated by

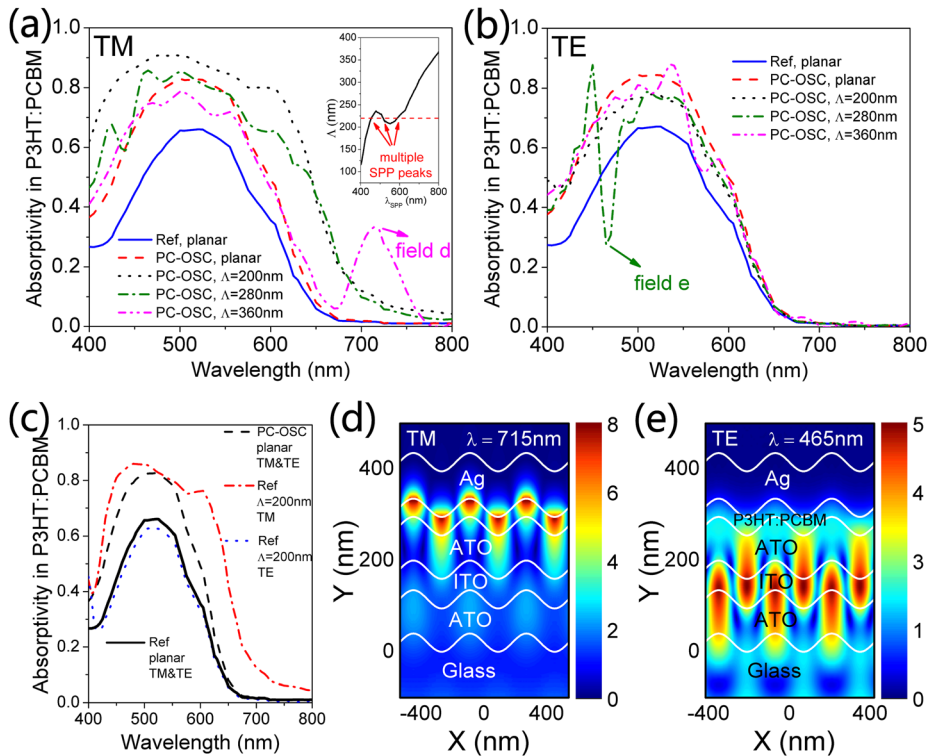


FIG. 3. Simulated absorptivity spectra in the P3HT:PCBM layer of the corrugated PC-OSC with various grating periods for normal (a) TM- and (b) TE-polarized incidence. (c) Comparison of the absorptivity spectra for the planar PC-OSC and corrugated reference OSC with a period of 200 nm, as they exhibit almost the same overall absorptivity. (d) Simulated TM-polarized field amplitude distributions in the PC-OSC with $\lambda = 715$ nm and $\Lambda = 360$ nm. (e) Simulated TE polarized field amplitude distributions in the PC-OSC with $\lambda = 465$ nm and $\Lambda = 280$ nm.

the E_z field amplitude distributions in Fig. 3(e). Thus from the discussion above, a proper period (e.g., 200 nm) should be chosen for improving the overall absorptivity of the corrugated PC-OSC, in consideration of both the excitation of multiple SPP peaks for TM polarization and the prevention of unexpected waveguide modes for TE polarization.

Finally, we calculate the TM, TE, and overall absorptivity of the corrugated devices with the variation of grating period in Fig. 4. The red and blue colors represent the results of the PC-OSC and the reference OSC, respectively. The dashed lines show the overall absorptivity of the aforementioned planar structures, while the squares, triangles, and circles give the A_{TM} , A_{TE} , and A_{Total} of the corrugated structures, respectively. It is noted that the performance of the PC-OSC is better than the reference OSC in all aspects, including the comparisons of planar and corrugated cases. With a proper

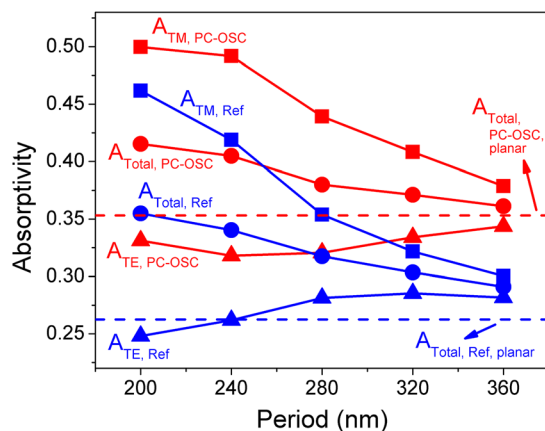


FIG. 4. Calculated absorptivity of the planar (dashed line) and corrugated (symbol) structures. The red and blue colors represent the results of the PC-OSC and the reference OSC, respectively. The squares, triangles, and circles give the A_{TM} , A_{TE} , and A_{Total} of the corrugated structures with various grating periods, respectively.

chosen period of 200 nm, the corrugated PC-OSC exhibits an overall absorptivity of 0.415, which is 58%, 18%, and 17% higher than the planar reference OSC, planar PC-OSC and corrugated reference OSC with the same period, respectively. Remarkably, the overall absorptivity of the planar PC-OSC (~ 0.353) is nearly the same as that of the corrugated reference OSC (~ 0.355) with the period of 200 nm, with their absorptivity spectra shown in Fig. 3(c). We observe the superiority of the PC-OSC that the absorption can be enhanced for both TM- and TE-polarized incidence compared with the planar reference OSC. However, the absorption in the corrugated reference OSC can only be enhanced for TM-polarized incidence. In fact, the planar PC-OSC is easier to be fabricated. Therefore, the PC based devices show potential value in thin-film solar cells. In experiment, a poly(3,4-ethylenedioxythiophene)-poly(styrenesulfonate) (PEDOT:PSS) layer may be inserted between the ATO layer and the active layer for a better electrical performance. Such layer would possibly affect the total absorptivity due to a red shift of the OTS wavelength. But we stress that it can be compensated by redesigning the lattice parameters of the PC.

In summary, we have proposed a design of planar PC-OSC that exhibits a broad-band absorption enhancement partly owing to the abnormal RI variation of P3HT:PCBM. The overall absorptivity exhibits an enhancement of $\sim 35\%$ compared with that of the optimized conventional planar OSC, and nearly the same as that of the conventional corrugated OSC with an optimized period of 200 nm. We expect that the present design strategy can also be applied to other optoelectronic devices, such as OLEDs. In particular, our design strategy is more applicable to small molecules based heterojunction OSCs,^{5,7} whose active layers are required to be very thin.

The authors thank Dr. Xian-Shu Luo for his valuable discussions and acknowledge the support from NSFC (Grant Nos. 90923037, 61137001, 61107024, and 61177090).

- ¹G. Li, V. Shrotriya, J. Huang, Y. Yao, T. Moriarty, K. Emery, and Y. Yang, *Nat. Mater.* **4**, 864 (2005).
- ²J. Y. Kim, K. Lee, N. E. Coates, D. Moses, T. Q. Nguyen, M. Dante, and A. J. Heeger, *Science* **317**, 222 (2007).
- ³A. K. K. Kyaw, X. W. Sun, C. Y. Jiang, G. Q. Lo, D. W. Zhao, and D. L. Kwong, *Appl. Phys. Lett.* **93**, 221107 (2008).
- ⁴M. Agrawal and P. Peumans, *Opt. Express* **16**, 5385 (2008).
- ⁵M. A. Sefunc, A. K. Okyay, and H. V. Demir, *Appl. Phys. Lett.* **98**, 093117 (2011).
- ⁶A. Williamson, É. McClean, D. Leipold, D. Zerulla, and E. Runge, *Appl. Phys. Lett.* **99**, 093307 (2011).
- ⁷C. Min, J. Li, G. Veronis, J. Y. Lee, S. Fan, and P. Peumans, *Appl. Phys. Lett.* **96**, 133302 (2010).
- ⁸Y. H. Su, Y. F. Ke, S. L. Cai, and Q. Y. Yao, *Light: Sci. Appl.* **1**, e14 (2012).
- ⁹B. Niesen, B. P. Rand, P. V. Dorpe, D. Cheyns, L. M. Tong, A. Dmitriev, and P. Heremans, "Plasmonic efficiency enhancement of high performance organic solar cells with a nanostructured rear electrode," *Adv. Energy Mater.* (published online).
- ¹⁰X. L. Zhang, J. Feng, J. F. Song, X. B. Li, and H. B. Sun, *Opt. Lett.* **36**, 3915 (2011).
- ¹¹M. Kaliteevski, I. Iorsh, S. Brand, R. A. Abram, J. M. Chamberlain, A. V. Kavokin, and I. A. Shelykh, *Phys. Rev. B* **76**, 165415 (2007).
- ¹²D. P. Puzzo, M. G. Helander, P. G. O'Brien, Z. Wang, N. Soheilnia, N. Kherani, Z. Lu, and G. A. Ozin, *Nano Lett.* **11**, 1457 (2011).
- ¹³A. J. Moule and K. Meerholz, *Appl. Phys. Lett.* **91**, 061901 (2007).
- ¹⁴J. K. Kim, T. Gessmann, E. F. Schubert, J. Q. Xi, H. Luo, J. Cho, C. Sone, and Y. Park, *Appl. Phys. Lett.* **88**, 013501 (2006).
- ¹⁵J. Feng, T. Okamoto, and S. Kawata, *Opt. Lett.* **30**, 2302 (2005).
- ¹⁶J. Feng, T. Okamoto, R. Naraoka, and S. Kawata, *Appl. Phys. Lett.* **93**, 051106 (2008).
- ¹⁷X. L. Zhang, J. F. Song, G. Q. Lo, and D. L. D Wong, *Opt. Express* **18**, 22462 (2010).
- ¹⁸R. H. Raether, *Surface Plasmons on Smooth and Rough Surfaces and on Gratings* (Springer, 1988).